Diffusion Magnetic Resonance Imaging and Fiber Tractography

The State of the Art and its Potential Impact on Patient Management

Sjoerd B. Vos, MSc*, Chantal M.W. Tax, MSc,
Alexander Leemans, PhD

KEYWORDS

• White matter • Diffusion-weighted MRI (DWI) • Diffusion tensor MRI (DTI) • Fiber tractography
• High angular resolution diffusion imaging (HARDI)

KEY POINTS

- Diffusion magnetic resonance (MR) imaging can characterize microstructural properties of brain tissue based on the random motion of water molecules.
- With diffusion tensor imaging (DTI), valuable quantitative measures can be calculated, such as the magnitude and anisotropy of diffusion.
- Fiber tractography allows for the three-dimensional reconstruction of the tissue architecture such as the trajectories of white matter fiber bundles.
- State of the art diffusion MR imaging approaches beyond DTI can provide more reliable information on the microstructural and architectural tissue organization.
- Clinical uses of diffusion MR imaging include the detection of microstructural abnormalities and the virtual reconstruction of fiber pathways for surgical planning.

INTRODUCTION TO DIFFUSION TENSOR MAGNETIC RESONANCE IMAGING

From Diffusion to Diffusion-Weighted Magnetic Resonance Imaging

To introduce diffusion-weighted magnetic resonance imaging (DWI), we must go back to the nineteenth century. In 1827, Robert Brown observed random motion of pollen particles suspended in water.[1] All molecules in a fluid warmer than absolute zero temperature inherently have thermal energies that cause them to show random motions: a phenomenon now known as Brownian motion. Later, Albert Einstein described this physical process theoretically with the well-known diffusion equation as follows[2]: $\langle x^2 \rangle = 2Dt$. Here, $\langle x^2 \rangle$ denotes the mean squared displacement in 1 dimension, D is the diffusion coefficient of the solution, and t is the diffusion time. So, for a certain value for D, the longer a group of molecules is allowed to move, the larger the spread of these molecules is. In this example, the medium in which particles diffuse is assumed to be homogeneous. In such cases, the mean squared displacement $\langle x^2 \rangle$ is independent of the direction in which particles move (hence, isotropic diffusion), as shown in **Fig. 1**A. If the medium is inhomogeneous (ie, structured in some way), diffusion is not equal in all directions (hence, anisotropic diffusion) (see **Fig. 1**B).

None of the authors has a financial conflict of interest.
Image Sciences Institute, University Medical Center Utrecht, Heidelberglaan 100, Utrecht 3584 CX, The Netherlands
* Corresponding author.
E-mail address: sjoerd@isi.uu.nl

PET Clin 8 (2013) 279–293
http://dx.doi.org/10.1016/j.cpet.2013.04.002
1556-8598/13/$ – see front matter

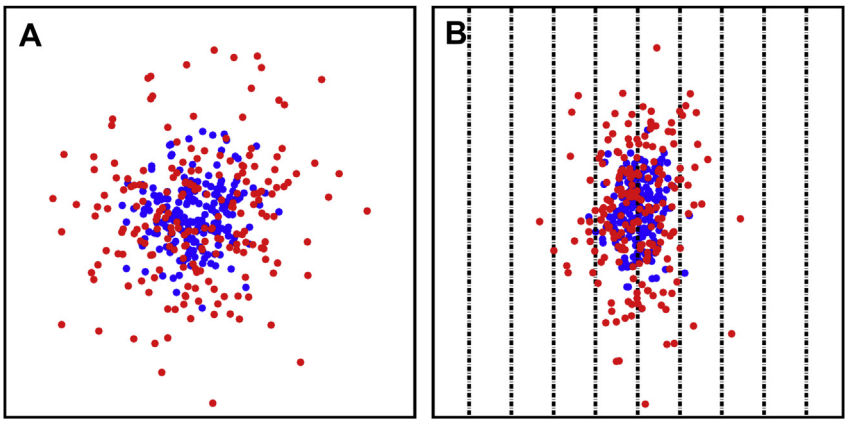

Fig. 1. (*A*) The blue and red dots visualize the displacement of 200 particles over a certain time t (*blue dots*) and 2t (*red dots*). (*B*) Semipermeable barriers, as indicated by the dashed black lines, can hinder diffusion along one direction but not the other. This situation results in diffusion that is not equal in all directions, called anisotropic diffusion.

Diffusion not only takes place in pure fluids; it is also present in tissue that contains fluid particles, such as the brain (more than 75% of the brain consists of water molecules). The brain consists of roughly 100 billion (10^{11}) neurons,[3] and each neuron has a complex cell structure (including cytoskeletal filaments, membranes, a myelin sheath, and so forth) that hinders or restricts diffusion within and between these neurons. As a result, the diffusion medium in the brain is very inhomogeneous, making diffusion highly anisotropic.[4] For a comprehensive overview of the role of each cellular component in diffusion anisotropy, see Beaulieau.[5]

To use diffusion as an image contrast, the conventional magnetic resonance (MR) imaging signal (which originates from the water molecules) must be sensitized to diffusion. During MR imaging acquisition, several magnetic field gradients are applied to generate the images. An example of such an image (T2-weighted image) is shown in **Fig. 2**A. To generate a DW image, additional magnetic field gradients are used, which cause the signal to attenuate as a result of diffusion.[6,7] For a specific orientation of the diffusion gradient (eg, along the z-axis), only diffusion along this axis attenuates the signal. The anisotropic diffusion in the brain can be observed when acquiring DW images with different diffusion gradient directions (see **Fig. 2**B–D).[4]

It can also be appreciated that the diffusion process causes signal attenuation by looking at the

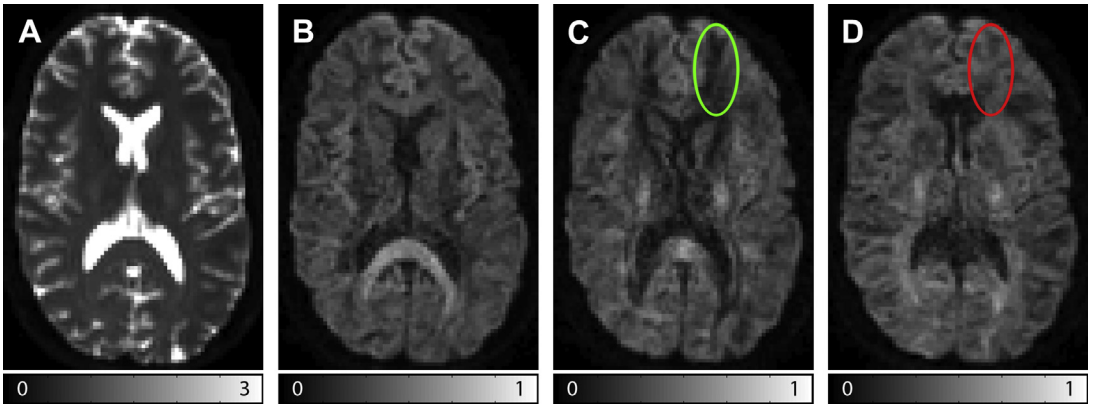

Fig. 2. Non-DW (*A*) and DW images with 3 different diffusion directions: (*B*) inferior-superior, (*C*) anterior-posterior, and (*D*) left-right. Throughout the brain, differences in contrast between the different diffusion directions can be observed, caused by anisotropic diffusion. The green and red ellipses (*C, D*) indicate regions of highly anisotropic diffusion. Diffusion causes signal attenuation, so regions of low intensity (eg, green ellipse in *C*) are caused by a high diffusivity along that direction, whereas hyperintense regions (eg, the red ellipse in *D*) are caused by a low diffusivity along that direction.

diffusion weighting in a more mathematical way. The signal equation for DW (S_{DW}) intensities is[8]

$$S_{DW} = S_0 \times e^{-TE/T2} \times e^{-bD} = S_{b0} \times e^{-bD} \quad [1]$$

where S_0 is the signal after excitation, $T2$ is the tissue-specific transverse relaxation time, TE is the time at which the signal echo is read out, b is the b value (ie, the magnitude of diffusion weighting), and D is the diffusion coefficient. When b = 0 s/mm^2, no diffusion weighting is applied, resulting in the T2-weighted image (see **Fig. 2**A), also called the non-DW image or b = 0 image.

In DWI, it is common to name the diffusion coefficient the apparent diffusion coefficient (ADC), because it reflects the estimated diffusion from MR measurements, not the true microstructural diffusion. From Eq. [1], the ADC can be quantified based on 1 DW and 1 non-DW measurement. The change in image contrast with b value is shown in **Fig. 3**.

Diffusion Tensor Magnetic Resonance Imaging

Diffusion is largest parallel to the orientation of brain fibers and smallest perpendicular to the fiber orientation.[4,6] Moseley and colleagues[4] suggested using this knowledge to determine fiber orientations from the MR measurements, but a generalized quantification was first described in 1994, when Basser and colleagues[9] proposed Diffusion Tensor magnetic Resonance Imaging (DTI). In DTI, the diffusion profile in each imaging voxel is modeled as a tensor, D:

$$D = \begin{bmatrix} Dxx & Dxy & Dxz \\ Dyx & Dyy & Dyz \\ Dzx & Dzy & Dzz \end{bmatrix} \quad [2]$$

Here, the diagonal components Dxx, Dyy, and Dzz are the ADC values in the x-direction, y-direction, and z-direction, and the off-diagonal components denote the correlations between the diagonal values. For instance, a high Dxy indicates a high correlation between diffusion in the x-direction and y-direction. Conceptually, D can be visualized as an ellipsoid, with its surface representing the probability distribution of the mean squared displacement (**Fig. 4**A). Because diffusion does not occur in a direction (eg, from x to −x) but along an axis (ie, in the orientation of axis x), it is impossible to distinguish between diffusion from −x to x and diffusion from x to −x, which means that Dxy and Dyx are equal (similarly, $Dxz = Dzx$ and $Dyz = Dzy$), and, hence, D is called a symmetric tensor. Because of this symmetry, there are only 6 unknown components in D. To estimate these 6 elements, at least 6 unique diffusion measurements are needed, meaning 6 DW images and 1 non-DW image. In addition, these 6 DW images must be acquired with gradient directions that are noncollinear (ie, orientationally independent of each other).

As seen in Eq. [2], the tensor describes the estimated diffusion profile based on the standard global coordinate system (x, y, z), as used in the MR scanner. This statement means that the values of the tensor elements in each voxel depend on the orientation of the object with respect to these axes. This situation is visualized in **Fig. 4**A, B, where the same tensor is oriented differently. Defining a local coordinate system for each voxel separately enables formulation of the tensor independent of the orientation of the tensor, as shown in **Fig. 4**C, D. With this coordinate transform, the DT can be defined by 3 perpendicular vectors, called eigenvectors, along which diffusion can be measured independently of the other orientations. The magnitudes of diffusion along these 3 eigenvectors (ε_1, ε_2, and ε_3) are called the eigenvalues (λ_1, λ_2, and λ_3). The eigenvectors and eigenvalues

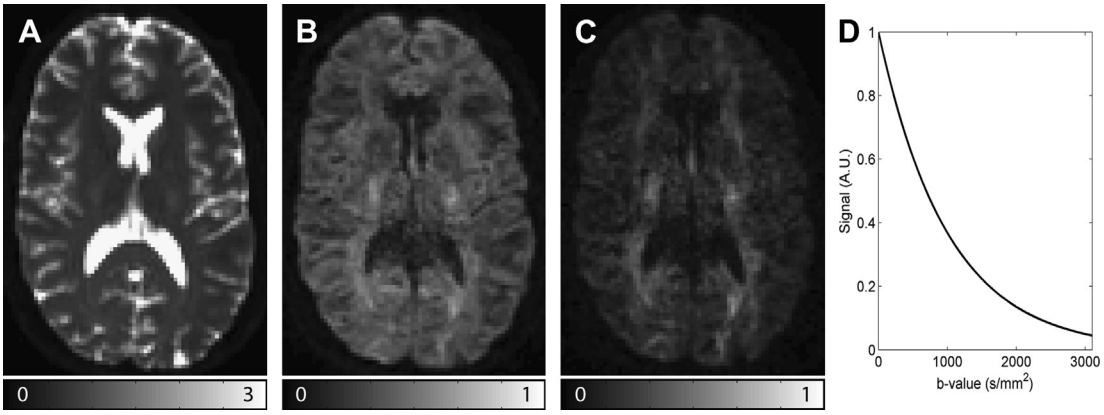

Fig. 3. (*A*) Non-DW image; (*B*) DW image with b = 1000 s/mm^2; (*C*) DW image with b = 2500 s/mm^2; (*D*) how signal decreases exponentially with the b value.

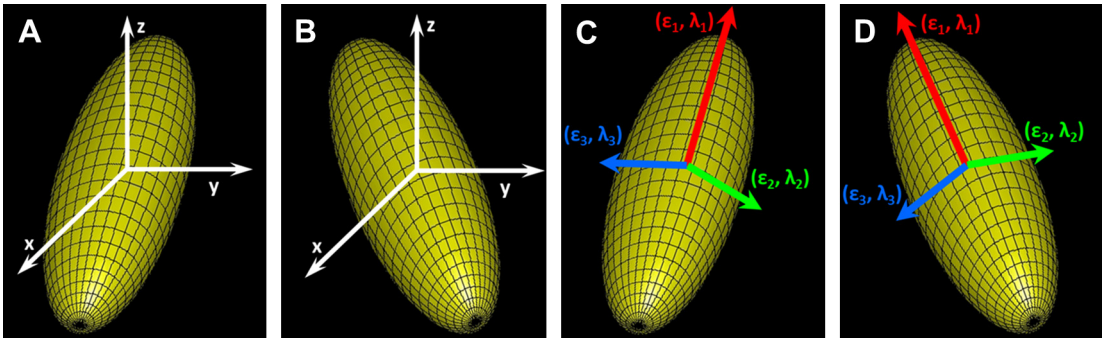

Fig. 4. The DT can be visualized as an ellipsoid, where the surface represents the surface of mean displacement. This situation means that at a given time t, there is equal probability of finding a diffused molecule anywhere on the surface. In a global coordinate system (*A, B*), each tensor component (eg, *Dxx*) is dependent on the orientation of the tensor. In a local coordinate system (*C, D*), the eigenvectors (ε_1–ε_3) and eigenvalues (λ_1–λ_3) describe the principal diffusion directions and their magnitudes, respectively.

are ordered such that the first eigenvector, ε_1, corresponds to the largest eigenvalue, λ_1. The first eigenvector is the orientation along which the diffusion is highest. Assuming that this dominant diffusion oriented is parallel to the fiber pathways, ε_1 reflects the main axis of these fiber trajectories.

DTI and quantitative measures

There are several scalar measures that can be extracted from the DT. In this section, the most popular DTI-based metrics are discussed. The mean diffusivity (MD, equal to the average of the 3 eigenvalues) describes the overall magnitude of the diffusion. In cerebrospinal fluid (CSF) regions, for instance, MD values are in the order of 3×10^{-3} mm^2/s. By contrast, the MD of brain white and gray matter is roughly 0.7×10^{-3} and 0.8×10^{-3} mm^2/s, respectively.[10] Another popular property of the DT is the degree of anisotropy with which diffusion occurs. Although there are several fractional anisotropy,[11] the most common measure is fractional anisotropy (FA), which represents the standard deviation of the eigenvalues, scaled between 0 (isotropic) and 1 (totally anisotropic).[12] Example images of these 2 DTI metrics are shown in **Fig. 5**A, B.

Changes in brain microstructure modulate both the magnitude and anisotropy of diffusion. For instance, Hanyu and colleagues[13] have shown that in Alzheimer disease, these diffusional changes can be observed before any abnormalities can be observed in conventional MR imaging (Alzheimer disease, and other diseases, are discussed in more detail later in this article). Despite being sensitive, it should be clear that changes in FA are not specific. For instance, a decrease in FA could be caused by either a decrease in λ_1, increases in λ_2 or λ_3, or both of these happening simultaneously.

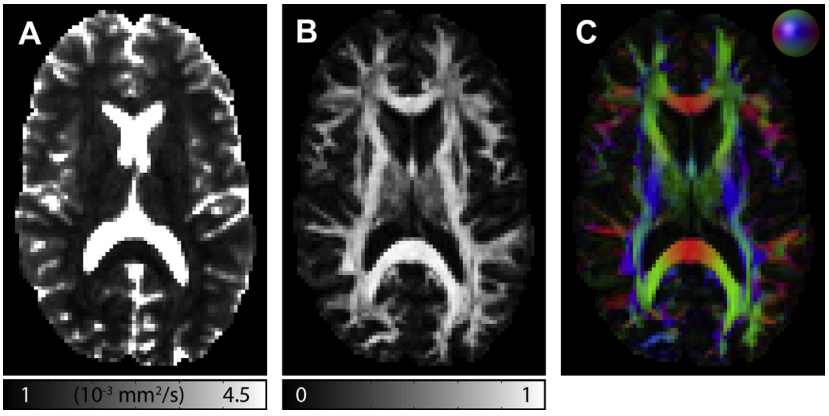

Fig. 5. (*A*) MD; (*B*) FA; and (*C*) diffusion-encoded-color (DEC) map. The DEC map in (*C*) is color encoded by the direction of the first eigenvector (ε_1), as indicated by the color index sphere in the top right: green indicates anterior-posterior; red means left-right; and blue is inferior-superior. The intensity in (*C*) is scaled by the FA, so that regions of low anisotropy, where ε_1 is less informative, have a lower intensity.

To further understand what is driving the diffusion anisotropy, 2 other DTI measures are often used: the axial diffusivity (ie, the diffusion parallel to the fiber orientation [$\lambda_{||} = \lambda_1$]) and the radial diffusivity (the average of the diffusivities perpendicular to the fiber [$\lambda_{\perp} = (\lambda_2 + \lambda_3)/2$]).[12,14]

The local fiber orientation can be visualized in a diffusion-encoded color (DEC) map (see **Fig. 5**C). In this map, the FA map is color encoded based on the orientation of largest diffusion, ε_1. In this DEC map, green indicates that ε_1 is oriented anterior-posterior, red means left-right, and blue is inferior-superior.

Fiber Tractography

The principal diffusion direction of the DT (ellipsoid) is given by ε_1 and can be calculated for each voxel. Plotting these first eigenvectors therefore yields a discrete representation of the main diffusion directions throughout the brain. This representation is shown in **Fig. 6**A and B, where diffusion ellipsoids (left hemisphere) and first eigenvectors (right hemisphere) are shown. From these voxel-wise glyph objects, or glyphs, the voxel-by-voxel continuity in the diffusion orientations can be appreciated. From the first eigenvectors at each voxel, continuous representations of the principal diffusion orientations can also be created. This virtual reconstruction of fiber tract pathways is called fiber tractography (FT) or fiber tracking.[15,16] Starting from a certain voxel within the brain, a fiber tract pathway can be created in a step-wise way by following ε_1 in each subsequent voxel. This fiber pathway (see **Fig. 6**C) gives a more continuous representation than the eigenvectors, resulting in a more intuitive representation of the data.

Reconstruction of fiber tracts throughout the brain, termed whole-brain tractography, is possible by tract propagation at each location (**Fig. 7**A–C). Although such a set of fiber tracts may seem a big tangle, it can be disentangled with a priori anatomic knowledge of the location of specific fiber bundles. For instance, postmortem anatomic studies have shown that the arcuate fasciculus connects the language areas of Broca and Wernicke.[17,18] Identification of these areas can guide us to select the pathways of the arcuate fasciculus (**Fig. 7**D–F).[19,20]

Analysis of DTI Data

Analysis of DTI data, for instance to compare diffusion measures between healthy controls and individuals with some disease, can be performed in multiple ways, in which each method has its own specific benefits and drawbacks.[21] A short overview is given here of the most widely used approaches; for a more extensive overview, the interested reader is referred to Ref.[22]

Region-of-interest analysis

When interested in a specific white matter (WM) bundle or region, manually delineating a region of interest (ROI) allows for the calculation of diffusion statistics within this ROI. When drawing an ROI on each subject's DTI scan, a comparison between subjects can be made.[23] The need for manual ROI delineation makes this a time-consuming method, especially when one is interested in many different regions or in large-cohort studies. Moreover, it is user subjective and therefore poorly reproducible.

Atlas-based analysis

Instead of manual ROI placement, a predefined atlas with each brain region pre-segmented can also be used, to register each subject to this atlas image. In this way, the brain can be automatically parcellated and average DTI metrics for each

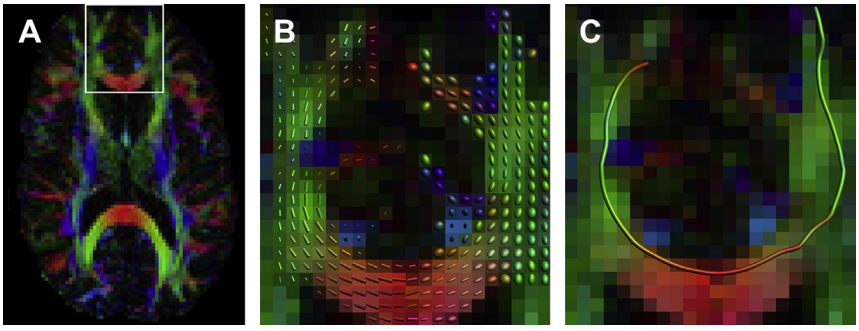

Fig. 6. (*A*) Axial slice of a DEC map. Enlargement of the genu of the corpus callosum outlined in (*A*) is shown in (*B, C*). (*B*) Tensors properties are visualized as voxel-wise glyph objects: the diffusion ellipsoid for the left hemisphere; the first eigenvectors (ε_1), shown as tubes, for the right hemisphere. Like the DEC map, the glyphs are colored by the orientation of ε_1. From these discrete representations, fiber tractography can be used to generate a continuous fiber tract pathway, shown in (*C*).

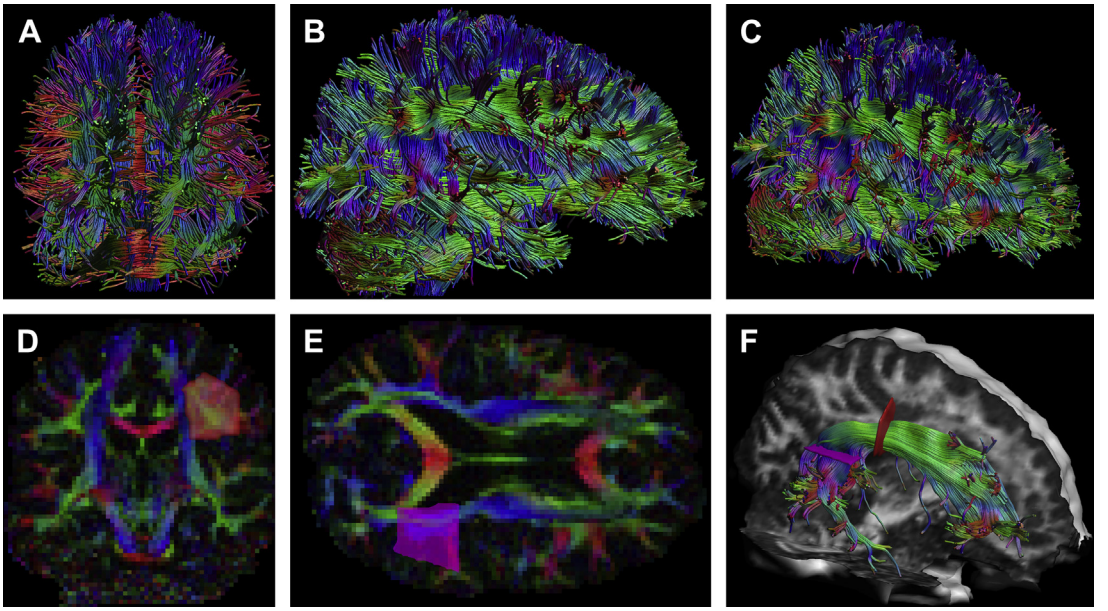

Fig. 7. Whole-brain tractography results shown from a coronal (*A*), sagittal (*B*), and oblique (*C*) angle. By delineating 2 regions of interest (ROIs) around the known locations of a specific white matter fiber bundle, only those reconstructed tract pathways are selected that intersect both these regions. For the left arcuate fasciculus, a coronal (*D*) and axial (*E*) ROI are sufficient to select the whole bundle (*F*), shown in the same orientation as (*C*).

region can be calculated.[24] As an automated and objective method, it does not suffer from many of the limitations of the ROI-based approach. However, large anatomic differences between atlas image and subject population (eg, caused by disease) may limit the reliability and accuracy of the method.[25]

Voxel-based analysis

Voxel-based analysis (VBA) is an automated approach in which scans from all subjects are coregistered for anatomic correspondence between subjects, and then compared on a voxelwise basis.[26] The extent of smoothing, required to compensate for residual misregistration between subjects, has a strong influence on the results, complicating the interpretation of VBA results.[27] Tract-based spatial statistics[28] was proposed as an alternative to ameliorate the drawbacks of VBA and is now one of the most popular methods for voxel-based analyses of DTI data, even although it has shortcomings of its own.[29,30]

FT analysis

Manual delineation of ROIs can also be used to select fiber tracts, as explained in **Fig. 7**. The DTI parameters can be averaged over all voxels within that selected tract, yielding more anatomically specific averages than the ROI-based analysis. Instead of manual ROI delineation to select tracts in each subject individually, it is also possible to do this in a (semi-) automated way,[31] strongly reducing the manual effort required at the possible expense of reduced accuracy/precision.

FROM DTI TO STATE OF THE ART DIFFUSION MR IMAGING

The cellular components that hinder the diffusion, and thus cause the diffusion contrast, include the cell membranes and myelin sheaths around the axons, which have a size in the order of microns.[5] The standard MR imaging voxel in DTI has dimensions in the order of millimeters, a difference in length scale of 10^3 with the diffusion that it aims to estimate. The tensor framework is based on the assumption that the diffusion profile in each imaging voxel can be characterized with a Gaussian distribution (ie, the DT). However, in voxels with multiple fiber populations (eg, fibers crossing within a voxel) or multiple fiber orientations (eg, bending fibers), the diffusion signal can no longer be described accurately by the DT,[32] as shown in **Fig. 8**. This intravoxel heterogeneity causes 2 main problems: (1) with more than 1 fiber population or orientation in a voxel, the principal diffusion direction no longer corresponds to the underlying fiber orientation[33]; and (2) the quantitative metrics derived from DTI do not reflect the measured diffusion profile in an accurate

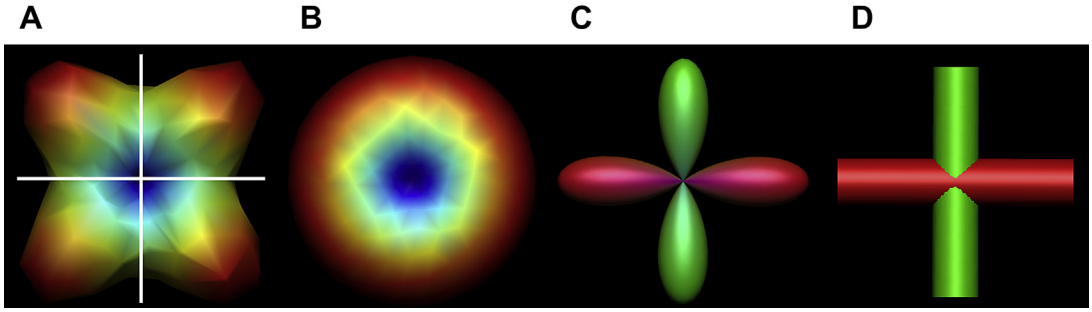

Fig. 8. Simulation of 1 voxel with 2 fiber populations crossing orthogonally in the image plane (orientations indicated by the white lines in *A*). Because of the invalid assumption in DTI, the ADC profile of the tensor (*B*) does not match the true ADC profile calculated directly from the diffusion signals (*A*). In these figures, low ADC is indicated in blue and high ADC in red. The resulting first eigenvector of the tensor is ill defined: depending on the noise, ε_1 is oriented somewhere in the image plane. When calculating the orientation distribution function (ODF) using more advanced models (*C*), the peaks of the ODF ideally represents the fiber orientations (*D*).

way.[34–36] With high percentages of WM voxels estimated to contain 2 or more fiber populations,[37,38] there is a need to go beyond the tensor model to characterize the diffusion profiles in a more reliable manner.

High Angular Resolution Diffusion Imaging

Among the first to propose alternative acquisition and signal estimation methods were Frank[39] and Tuch and colleagues.[40] Commonly known under the term high angular resolution diffusion imaging (HARDI), these techniques used a higher number of DW directions (eg, around 40 or more) to sample the three-dimensional (3D) diffusion attenuation profile at a higher angular resolution. From the measured diffusion signal, a 3D distribution of diffusion directions can be calculated, called the orientation distribution function (ODF). This ODF has its maxima along the orientations of the underlying fiber populations.

In recent years, a multitude of HARDI methods have been proposed to reconstruct the ODF from the diffusion signal. The methods can be divided into 2 main groups: parametric and nonparametric methods. The technique initially proposed by Tuch and colleagues,[40] Q-ball imaging (QBI), is a nonparametric approach, in which a mathematical approximation converts the diffusion signal to the diffusion ODF[41] (dODF). The *q*-value is another feature to describe the diffusion weighting (closely related to the *b*-value), on which the name QBI is based. The parametric methods are originally based on modeling the signal attenuation profile for a single fiber population, and the assumption that the measured signal attenuation profile can then be represented as a sum of these single fiber profiles.[39] One example of this method is spherical deconvolution, in which a single fiber response function can be used to deconvolve the diffusion signal to obtain the fiber ODF[42] (fODF), as shown in **Fig. 9**. This response function can

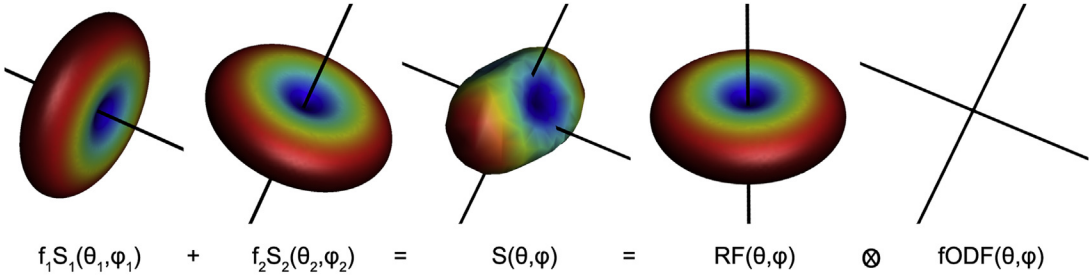

Fig. 9. Example of spherical (de-) convolution. Two fiber populations with different orientations are shown as black lines, with the corresponding DW signals, $S_1(\theta_1,\varphi_1)$ and $S_2(\theta_2,\varphi_2)$, and equal volume fractions ($f_1 = f_2 = 0.5$). In the DW profiles, low signal is indicated in blue and high signal in red. The combined diffusion signal is shown in the middle, $S(\theta,\varphi)$. $S(\theta,\varphi)$ can also be expressed as a single fiber response function, with $RF(\theta,\varphi)$ characterizing the diffusion signal of a single fiber, and convoluted (indicated by ⊗) with an $fODF(\theta,\varphi)$. In diffusion imaging, the measured signal $S(\theta,\varphi)$ can be deconvoluted with the RF to obtain the fODF.

be estimated from the diffusion signal in regions with a single fiber population.

Using the ODFs from these advanced techniques, multi-fiber tractography uses the peak orientations obtained from the ODFs (**Fig. 8**C, D), as an alternative to the first eigenvector obtained from DTI. Fillard and colleagues[43] and Jeurissen and colleagues[44] have shown that multi-fiber tractography can be used to track through regions of multiple fiber populations, as shown by the simulation in **Fig. 10**.

The ODFs calculated using parametric and nonparametric methods differ. An important difference between parametric and nonparametric methods is that the fODF obtained from spherical deconvolution methods is an absolute measure, in which the size and shape of fODF peaks of different fiber populations within a voxel are independent of each other. This situation has led to the definition of quantitative measures based on the fODF: the apparent fiber density[45] and the hindrance modulated orientational anisotropy.[46] These are scalar values that characterize the diffusion properties for each detected fiber population per voxel. By contrast, the dODF is normalized to have unit probability over the sphere, and the dODF amplitude of 1 peak is therefore dependent on the presence and size of other populations, making it difficult to define similar metrics.

Alternative Diffusion MR Imaging Approaches

Several other approaches have been proposed to describe the measured diffusion signals. Diffusion spectrum imaging[47] (DSI) uses many different *q* values along a high number of directions to fill a 3D Cartesian grid in q-space. The k-space (used in MR image generation) samples the spatial positions of the signal. Similar for the k-space and image space, the Fourier transform is a direct mathematical relation between the q-space and the probability density of diffusion. However, to fill the entire q-space, many more DW images are required and at higher *q* values, putting high demands on scan time for clinical MR systems, resulting in a low use of DSI in (pre-) clinical diffusion MR studies.

Another alternative is diffusion kurtosis imaging[48] (DKI), already extensively used in clinical and preclinical research studies.[49,50] The kurtosis is a measure of how non-Gaussian the diffusion is. Full quantification of the anisotropic kurtosis is achieved by estimating the kurtosis tensor, requiring at least 15 diffusion directions and 2 nonzero *b* values, which can be acquired clinically in acquisition times as low as 5 minutes.

More specific modeling of different tissue components to describe the signal attenuation profile was proposed by Assaf and colleagues[51] and dubbed CHARMED (the composite hindered and restricted model of diffusion). Here, the volume fractions as well as diffusion properties of the hindered (eg, extra-axonal space) and restricted (eg, intra-axonal space) components are estimated, and any observed diffusion changes can therefore be interpreted with a higher specificity. More recently, models have been proposed to estimate axonal diameters and densities in the brain, with initial findings showing strong differences between the genu, midbody, and splenium of the corpus callosum.[52]

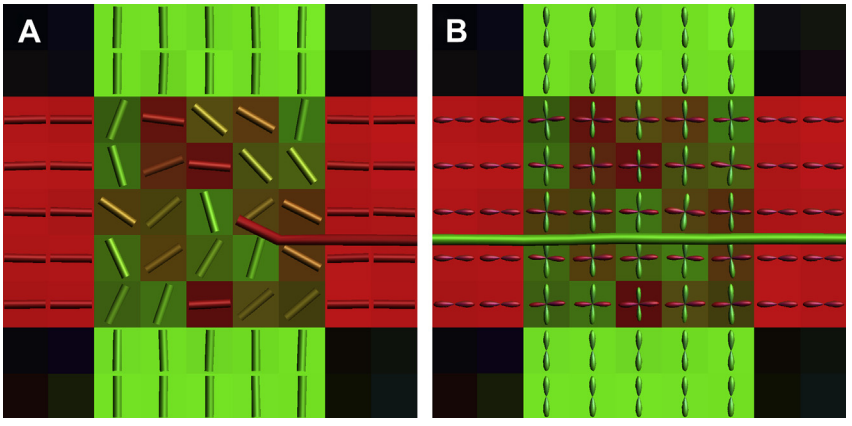

Fig. 10. Simulation of 2 individual fiber populations crossing at a 90° angle. (*A*) The first eigenvectors, ε_1; and (*B*) the ODFs in this region. At such crossings, the ε_1s do not reflect the underlying fiber architecture (*A*). FT through such a region of a crossing is therefore unreliable. The tract terminates at the region of crossing fibers because the angular deviation is too large. The ODFs (*B*) are more robust, and can be used more reliably to perform tractography.

CLINICAL AND PRECLINICAL USE OF DIFFUSION MR IMAGING

The role of DWI is well established in clinical practice, for example in stroke,[53] and radiotherapy treatment evaluation.[54] There are a myriad of brain diseases, with different physiologic underpinnings, which all cause changes in tissue organization and diffusion properties. This diversity means that there is a huge potential for the use of diffusion MR imaging. DTI and more advanced diffusion MR imaging methods are being used extensively in clinical research studies, with most studies comparing DTI parameters like FA and MD between patients and controls, trying to correlate these changes with clinical parameters. However, the use of diffusion MR imaging in clinical practice (ie, on a patient-by-patient basis) is still limited. The next section focuses on a few applications to show its potential for clinical use in more detail.

Alzheimer Disease

In Alzheimer disease, patients initially have deficits in mental functioning like emotional behavior, perception, and memory. Neurons and synapses in the cerebral cortex and subcortical regions degrade, which results in atrophy of the affected structures.[55] Diffusion MR imaging can detect these changes in WM microstructure and can give insight in the type of microstructural damage by looking at changes in MD and FA.[56] Traditional biomarkers such as CSF levels of tau protein and amyloid β_{42} are good diagnostic predictors of conversion from mild cognitive impairment to Alzheimer disease. Recently, FA, MD, and the radial diffusivity have been shown to be even better predictors of disease progression in a small patient population.[57]

Parkinson Disease

Parkinson disease is characterized by tremor and difficulties in coordination and movement. Deep brain stimulation is a therapy that aims at improvement of the patient's motor function by electrical stimulation of the motor part of the subthalamic nucleus. Accurate localization of this part is of crucial importance, because wrong placement of the electrode in the limbic or associative part of the subthalamic nucleus leads to cognitive and emotional side effects in 50% of the patients. Researchers have used DTI and HARDI-based tractography to localize the motor part by looking at its connectivity with other motor areas.[58] This information can then be used by neurosurgeons for better targeting.

Stroke

DWI is very sensitive to early ischemic injury and shows increased signal intensity (and thus decreased signal intensity on ADC maps), and is clinically used for lesion examination. DTI measures might provide more insight in the pathology of stroke, compared with the ADC alone. For instance, FA has been shown to correlate with recovery from stroke, decreasing in correspondence to Wallerian degeneration[33] and sometimes increasing as a result of WM reorganization.[59]

Cancer

Diffusion MR imaging, together with other modalities, can be used in the characterization of tumor tissue. Recently, DKI has been shown to have strong discriminative power to distinguish high-grade from low-grade gliomas in the brain.[50]

Alternatively, DTI is sensitive to microstructural changes after cancer treatment. After chemotherapy treatment of breast cancer, patients experienced cognitive deficits that were correlated with lower FA values in the corpus callosum.[60] In whole-brain VBA studies, changes in FA and MD were detected in patients (compared with controls) throughout the brain, with larger changes in patients with cognitive impairment.[61,62] Concomitant changes in radial diffusivity observed in these studies indicate that myelin degradation is the most likely underlying cause.[14,21] These studies conducted cross-sectional analyses, comparing posttreatment patients with controls. In the first longitudinal study, in which patients who have breast cancer were examined before and 3 to 4 months after treatment, Deprez and colleagues[63] showed that these patients show cognitive decline after treatment, which is strongly correlated with decreased FA in large areas of the WM. Whether these changes remain during years after treatment is still unclear, and strongly depends on the type and dose of the chemotherapeutic agents used in treatment. For an extensive review of chemotherapy-induced changes, the interested reader is referred to Deprez and colleagues.[21]

Traumatic Brain Injury

Whereas conventional MR imaging contrasts (eg, T1-weighted or T2-weighted images) have great use in assessing the acute phase of lesions in patients with traumatic brain injury, DTI has the potential to detect more subtle changes throughout the WM in the subacute or chronic phases, showing axonal injury whereas T1-weighted and T2-weighted images show no change (eg, Arfanakis and colleagues[64]). More

detailed investigations have shown that FA is correlated with parameters that indicate clinical severity of the injury.[65] This diffuse brain damage can result in long-term behavioral and cognitive changes, which are associated with changes in DTI parameters.[66] Similar changes can be observed in children and adolescents, with FA and MD in motor pathways correlated with movement control and processing of visual stimuli.[67,68] As a result, DTI measures such as FA may provide an important noninvasive marker of microstructural injury to predict clinical outcome of patients.[69,70]

Epilepsy

Epilepsy is a common neurologic disorder characterized by seizures caused by temporary abnormal brain activity, which can include tonic-clonic phases, loss of consciousness, or change in behavior. Case studies performed between seizures (interictal) show that putative epileptogenic areas and connected brain regions show increased MD and reduced FA values.[71] However, it is not clear whether this finding is cause or effect, and the value of DTI in this evaluation still has to be investigated in more detail.

Tractography in particular can be used to investigate structural abnormalities in patients with epilepsy and has been applied to map epileptogenic networks, revealing structural connections of the epileptic focus with other brain regions. Connections of the medial temporal lobe to the cerebellum and frontal and occipital lobes, for example, may explain seizure characteristics seen in temporal lobe epilepsy, like motor automatisms and auras.[72] Hippocampal sclerosis is the most commonly found cause of temporal lobe epilepsy, and DTI tractography analysis has indicated chronic structural changes (reduction in FA) in the cingulum, fornix, and corpus callosum, suggesting a network of structural changes instead of involvement of only the hippocampus.[73] However, differences in connectivity found in patients with epilepsy have to be interpreted with care, because there is no reference to validate these findings.

Neurosurgery

Since the early development of diffusion MR imaging, the potential of tractography in neurosurgical planning has been evident. Complete removal of the lesion is the primary goal of neurosurgery, but it is important not to cause too much functional damage during surgery, which can worsen the situation of the patient. The position of nearby fiber tract pathways can be visualized relative to the lesion,[74] as shown in **Fig. 11**. The arcuate fasciculus, for instance, is an important WM tract in the language network, and is often subject to investigation in neurosurgical applications. Alternatively, reconstruction of the optic radiation is important in temporal lobe epilepsy surgery, because the anterior extent is often located in the resection area, and damage to that bundle can lead to loss of vision.[75] For these reasons, use of fiber tracking in preoperative planning may improve postsurgical outcome.[76]

In these applications, the reliability and reproducibility of the reconstructed pathways are essential (eg, Kristo and colleagues[77]). The DT model is inaccurate at regions of crossing fibers, and it is therefore important to incorporate more advanced diffusion MR imaging methods. Tractography based on HARDI methods was shown to have improved results, both in the presence of tumors[78] and in treatment target localization.[58] Subsequent integration in neuronavigation systems is promising, but faces challenges like intraoperative brain shift. Diffusion MR imaging can also be combined with functional MR imaging, or other imaging modalities, to map both structure and function before neurosurgery (see Sherman and colleagues[79] for an overview).

FUTURE OUTLOOK OF THE STATE OF THE ART IN DIFFUSION MR IMAGING

DTI is still the most popular approach in diffusion MR imaging. The main reasons are its conceptual simplicity, possibility of extracting intuitive and quantitative scalar diffusion measures, such as FA and MD, and the short acquisition times (in the order of a few minutes). In the following sections, some critical considerations for the use of diffusion MR imaging are discussed, and an outlook over future uses of diffusion MR imaging in clinical settings is presented.

Diffusion MR Imaging Acquisition

Many DW images must be acquired to most accurately measure the DW signal and estimate the diffusion, especially for the advanced methods. Single-shot echo-planar imaging (SS-EPI) is the fastest method for MR image acquisition, and is therefore the method of choice for DWI. However, this acquisition speed comes at the cost of several drawbacks. SS-EPI is prone to susceptibility artifacts, which cause image deformations, which leads to a mismatch between the image and the anatomy it should represent. Second, higher image resolution reduces signal-to-noise ratio and increases these geometric distortions. Even with the use of parallel imaging techniques, which speed

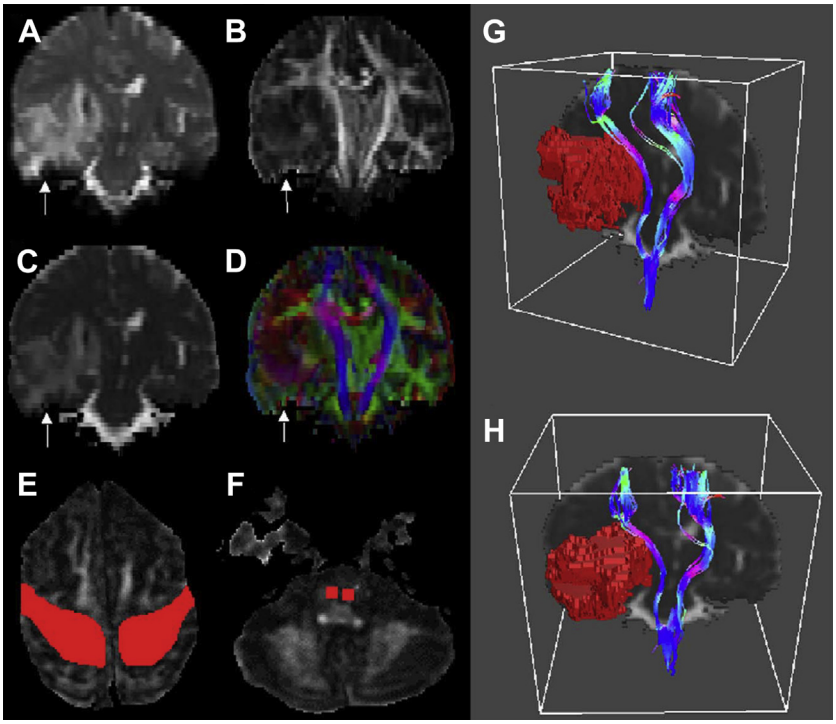

Fig. 11. Coronal images and FT results in a tumor patient. (*A*) T2-weighted image; (*B*) FA image; (*C*) MD image; (*D*) DEC image. In these images, the white arrow indicates the tumor. Tractography was initiated from the motor cortex (*red areas in E*) and the brain stem (*red overlay in F*). The corticospinal tracts connecting these 2 regions are shown in (*G, H*), with the tumor volume shown in red. (*Reproduced from* Clark CA, Barrick TR, Murphy MM, et al. White matter fiber tracking in patients with space-occupying lesions of the brain: a new technique for neurosurgical planning? Neuroimage 2003;20:1603. Fig. 2; with permission.)

up imaging and ameliorate these issues, distortions are still pronounced, with resolutions usually around $2 \times 2 \times 2$ mm or larger. Alternative imaging strategies have been proposed to address these drawbacks, but generally come at the cost of increased scan time, and are not so widely available (eg, Pipe and colleagues[80] and Holdsworth and colleagues[81]). For an extensive overview of these new methods, the interested reader is referred to Bammer and colleagues.[82]

Translating State of the Art Diffusion MR Imaging Approaches to the Clinic

The drawback of most of the advanced diffusion MR imaging methods (eg, DSI or axon diameter estimation) is the requirement for acquisition times that may be excessively long for clinical applications. To reduce acquisition times, these models can be simplified by fixing some of the parameters to be estimated, at the possible cost of less accurate estimates. An example of such a simplification is in the estimation of axonal diameters. Instead of estimating the full distribution of axonal diameters, the average axon diameter only can be estimated based on a shorter acquisition.[52] However, theoretically, disease may cause a broadening in the distribution without changing the average, which might be overlooked in the simplified model. Despite the challenges of translating the state of the art to clinical settings, these methods can provide more specific microstructural tissue properties in vivo, potentially yielding important new insights in microstructural pathologic changes.

Tractography

An important aspect in the use of tractography, especially in a clinical setting, is the accuracy of the reconstructed tracts. Diffusion hardware phantoms allow for an objective evaluation of tractography based on different diffusion MR imaging methods. Comparing tractography results with a ground truth, Fillard and colleagues[43] showed strong improvement in accuracy using multi-fiber versus tensor-based tracking. However, none of the investigated methods performed perfectly. Even although the multi-fiber tractography can track through fiber crossings, it is virtually impossible for tractography algorithms to distinguish

between fibers that cross or kiss within a voxel[83] (ie, populations that enter a voxel, but bend instead of crossing). Furthermore, there is no ground truth data set of the wiring of a human brain, which means it is challenging to quantify the accuracy of in vivo tractography. Despite these issues, technical as well as clinical research has already shown benefits of using ODF-based tractography.[43,58,76,78,84]

SUMMARY

Diffusion MR imaging is very sensitive to microstructural changes in tissue, and the DT model is commonly used to describe the orientational preference of diffusion. FA and MD values, which can be derived from the DT, have been shown to change in many neuropathologic conditions. For instance, in preclinical research studies into Alzheimer disease and traumatic brain injury, disease severity is found to correlate with FA. More advanced diffusion models like DKI or CHARMED can describe the diffusion more accurately than DTI, in turn providing more detailed information about the underlying tissue microstructure. In addition to microstructural tissue information, diffusion MR imaging can also provide a 3D architectural representation of the tissue using FT. DT tractography is used extensively in research settings to define WM fiber bundles and then extract FA or MD values from those tracts. Clinically, for instance, it is used in tumor resection, and several studies have shown improved outcome when incorporating it in presurgical planning. Diffusion MR imaging methods that can resolve crossing fibers, such as QBI, constrained spherical deconvolution, or DSI, are used in research studies to provide more accurate tractography results, and provide more feasible reconstructions of fiber tract pathways, especially in pathologic cases.

REFERENCES

1. Brown R. A brief account of microscopical observations made on the particles contained in the pollen of plants. Philosophical Magazine 1828;4: 161–73.
2. Einstein A. Über die von der molekularkinetischen Theorie der Wärme geforderte Bewegung von in ruhenden Flüssigkeiten suspendierten Teilchen. Ann Phys 1905;322:549–60 [in German].
3. Lange W. Cell number and cell density in the cerebellar cortex of man and other mammals. Cell Tissue Res 1975;157:115–24.
4. Moseley ME, Cohen Y, Kucharczyk J, et al. Diffusion-weighted MR imaging of anisotropic water diffusion in cat central nervous system. Radiology 1990;176:439–45.
5. Beaulieu C. The basis of anisotropic water diffusion in the nervous system–a technical review. NMR Biomed 2002;15:435–55.
6. Cleveland GG, Chang DC, Hazlewood CF, et al. Nuclear magnetic resonance measurement of skeletal muscle: anisotropy of the diffusion coefficient of the intracellular water. Biophys J 1976;16: 1043–53.
7. Le Bihan D, Breton E. Imagerie de diffusion in-vivo par resonance magnetique nucleaire. Compte Rendus de l'Académie des Sciences (Paris) 1985; 301:1109–12 [in French].
8. Stejskal EO, Tanner JE. Spin diffusion measurements: spin echoes in the presence of time-dependent field gradient. J Chem Phys 1965;42: 288–92.
9. Basser PJ, Mattiello J, Le Bihan D. MR diffusion tensor spectroscopy and imaging. Biophys J 1994;66:259–67.
10. Le Bihan D, Mangin JF, Poupon C, et al. Diffusion tensor imaging; concepts and applications. J Magn Reson Imaging 2001;13:534–46.
11. Pierpaoli C, Basser PJ. Toward a quantitative assessment of diffusion anisotropy. Magn Reson Med 1996;36:893–906.
12. Basser PJ. Inferring microstructural features and the physiological state of tissues from diffusion-weighted images. NMR Biomed 1995;8:333–44.
13. Hanyu H, Shindo H, Kakizaki D, et al. Increased water diffusion in cerebral white matter in Alzheimer's disease. Gerontology 1997;43:343–51.
14. Song SK, Sun SW, Ramsbottom MJ, et al. Dysmyelination revealed through MRI as increased radial (but unchanged axial) diffusion of water. Neuroimage 2002;17:1429–36.
15. Mori S, Brain BJ, Chacko VP, et al. Three-dimensional tracking of axonal projections in the brain by magnetic resonance imaging. Ann Neurol 1999;45:265–9.
16. Basser PJ, Pajevic S, Pierpaoli C, et al. In vivo fiber tractography using DT-MRI data. Magn Reson Med 2000;44:625–32.
17. Dejerine J. Anatomie de centres nerveux, vol. 1. Paris: Rueff et Cie; 1895 [in French].
18. Benson DF, Sheremata WA, Bouchard R, et al. Conduction aphasia: a clinicopathological study. Arch Neurol 1973;28:339–46.
19. Wakana S, Jiang H, Nagae-Poetscher LM, et al. Fiber tract-based atlas of human white matter anatomy. Radiology 2004;230:77–87.
20. Catani M, Jones DK, ffytche DH. Perisylvian language networks of the human brain. Ann Neurol 2005;57:8–16.
21. Deprez S, Billiot T, Sunaert S, et al. Diffusion tensor MIR of chemotherapy-induced cognitive

impairment in non-CNS cancer patients: a review. Brain Imaging Behav 2013. http://dx.doi.org/10.1007/s11682-012-9220-1. [Epub ahead of print].
22. Cercignani M. Strategies for patient-control comparison in diffusion MR data. In: Jones DK, editor. Diffusion MRI: theory, methods, and applications. Oxford, UK: Oxford University Press; 2011. p. 485–99.
23. Snook L, Paulson LA, Roy D, et al. Diffusion tensor imaging in neurodevelopment in children and young adults. Neuroimage 2005;26:1164–73.
24. Mori S, Oishi K, Jiang H, et al. Stereotaxic white matter atlas based on diffusion tensor imaging in an ICBM template. Neuroimage 2008;40:570–82.
25. Oishi K, Faria A, Jiang H, et al. Atlas-based whole brain white matter analysis using large deformation diffeomorphic metric mapping: application to normal elderly and Alzheimer's disease participants. Neuroimage 2009;46:486–99.
26. Ashburner J, Friston K. Voxel-based morphometry–the methods. Neuroimage 2000;11:805–21.
27. Jones DK, Symms MR, Cercignani M, et al. The effect of filter size on VBM analyses of DT-MRI data. Neuroimage 2005;26:546–54.
28. Smith SM, Jenkinson M, Johansen-Berg H, et al. Tract-based spatial statistics: voxelwise analysis of multi-subject diffusion data. Neuroimage 2006; 31:1487–505.
29. Van Hecke W, Leemans A, de Backer S, et al. Comparing isotropic and anisotropic smoothing for voxel-based DTI analyses: a simulation study. Hum Brain Mapp 2010;31:98–114.
30. Edden RA, Jones DK. Spatial and orientation heterogeneity in the statistical sensitivity of skeleton-based analyses of diffusion tensor MR imaging data. J Neurosci Methods 2011;201:213–9.
31. Lebel C, Walker L, Leemans A, et al. Microstructural maturation of the human brain from childhood to adulthood. Neuroimage 2008;40:1044–55.
32. Frank LR. Anisotropy in high angular resolution diffusion-weighted MRI. Magn Reson Med 2001; 45:935–9.
33. Pierpaoli C, Barnett A, Pajevic S, et al. Water diffusion changes in Wallerian degeneration and their dependence on white matter architecture. Neuroimage 2001;13:1174–85.
34. Alexander AL, Hasan KM, Lazar M, et al. Analysis of partial volume effects in diffusion-tensor MRI. Magn Reson Med 2001;45:770–80.
35. Vos SB, Jones DK, Viergever MA, et al. Partial volume effect as a hidden covariate in DTI analyses. Neuroimage 2011;55:1566–76.
36. Vos SB, Jones DK, Jeurissen B, et al. The influence of complex white matter architecture on the mean diffusivity in diffusion tensor MRI of the human brain. Neuroimage 2012;59:2208–16.
37. Behrens TE, Johansen-Berg H, Jbabdi S, et al. Probabilistic diffusion tractography with multiple fiber orientations: what can we gain? Neuroimage 2007;34:144–55.
38. Jeurissen B, Leemans A, Tournier JD, et al. Investigating the prevalence of complex fiber configurations in white matter tissues with diffusion magnetic resonance imaging. Hum Brain Mapp 2012. http://dx.doi.org/10.1002/hbm.22099. [Epub ahead of print].
39. Frank LR. Characterization of anisotropy in high angular resolution diffusion-weighted MRI. Magn Reson Med 2002;47:1083–99.
40. Tuch DS, Reese TG, Wiegell MR, et al. Diffusion MRI of complex neural architecture. Neuron 2003; 40:885–95.
41. Tuch DS. Q-ball imaging. Magn Reson Med 2004; 52:1358–72.
42. Tournier JD, Calamante F, Gadian DG, et al. Direct estimation of the fiber orientation distribution from diffusion-weighted MRI data using spherical deconvolution. Neuroimage 2004;23:1176–85.
43. Fillard P, Descoteaux M, Goh A, et al. Quantitative evaluation of 10 tractography algorithms on a realistic diffusion MR phantom. Neuroimage 2011;56: 220–34.
44. Jeurissen B, Leemans A, Jones DK, et al. Probabilistic fiber tracking using the residual bootstrap with constrained spherical deconvolution. Hum Brain Mapp 2011;32:461–79.
45. Raffelt D, Tournier JD, Rose S, et al. Apparent fibre density: a novel measure for the analysis of diffusion-weighted magnetic resonance images. Neuroimage 2012;59:3976–94.
46. Dell'Acqua F, Simmons A, Williams SC, et al. Can spherical deconvolution provide more information than fiber orientation? Hindrance modulated orientational anisotropy, a true-tract specific index to characterize white matter diffusion. Hum Brain Mapp 2012. http://dx.doi.org/10.1002/hbm.22080. [Epub ahead of print].
47. Wedeen VJ, Hagmann P, Tseng WY, et al. Mapping complex tissue architecture with diffusion spectrum magnetic resonance imaging. Magn Reson Med 2005;54:1377–86.
48. Jensen JH, Helpern JA, Ramani A, et al. Diffusional Kurtosis imaging: the quantification of non-gaussian water diffusion by means of magnetic resonance imaging. Magn Reson Med 2005;53:1432–40.
49. Fieremans E, Jensen JH, Helpern JA. White matter characterization with diffusional kurtosis imaging. Neuroimage 2011;58:177–88.
50. van Cauter S, Veraart J, Sijbers J, et al. Gliomas: diffusion kurtosis MR imaging in grading. Radiology 2012;263:492–501.
51. Assaf Y, Freidlin RZ, Rohde GK, et al. New modeling and experimental framework to characterize hindered and restricted water diffusion in the brain white matter. Magn Reson Med 2004;52:965–78.

52. Alexander DC, Hubbard PL, Hall MG, et al. Orientationally invariant indices of axon diameter and density from diffusion MRI. Neuroimage 2010;52: 1374–89.
53. Albers GW, Thijs VN, Wechsler L, et al. Magnetic resonance imaging profiles predict clinical response to early reperfusion; the DEFUSE study. Ann Neurol 2006;60:508–17.
54. Hermans R. Diffusion-weighted MRI in head and neck cancer. Curr Opin Otolaryngol Head Neck Surg 2010;18:72–8.
55. Fox NC, Scahill RI, Crum WR, et al. Correlations between rates of brain atrophy and cognitive decline in AD. Neurology 1999;52:1687–9.
56. Bozzali M, Falini A, Francheschi M, et al. White matter damage in Alzheimer's disease assessed in vivo using diffusion tensor magnetic resonance imaging. J Neurol Neurosurg Psychiatry 2002;72: 742–6.
57. Selnes P, Aarsland D, Bjornerud A, et al. Diffusion tensor imaging surpasses cerebrospinal fluid as predictor of cognitive decline and medial temporal lobe atrophy in subjective cognitive impairment and mild cognitive impairment. J Alzheimers Dis 2013;33:723–36.
58. Brunenberg EJ, Moeskops P, Backes WH, et al. Structural and resting state functional connectivity of the subthalamic nucleus: identification of motor STN parts and the hyperdirect pathway. PLoS One 2012;7:e39061.
59. van der Zijden JP, van der Toorn A, van der Marel K, et al. Longitudinal in vivo MRI of alterations in perilesional tissue after transcient ischemic stroke in rats. Exp Neurol 2008;212:207–12.
60. Abraham J, Haut MW, Moran MT, et al. Adjuvant chemotherapy for breast cancer: effects on cerebral white matter seen in diffusion tensor imaging. Clin Breast cancer 2008;8:88–91.
61. Deprez S, Amant F, Yigit R, et al. Chemotherapy-induced structural changes in cerebral white matter and its correlation with impaired cognitive functioning in breast cancer patients. Hum Brain Mapp 2011;30:480–93.
62. de Ruiter MB, Beneman L, Boogerd W, et al. Late effects of high-dose adjuvant chemotherapy on white and gray matter in breast cancer survivors: converging results from multimodal magnetic resonance imaging. Hum Brain Mapp 2011;33: 2971–83.
63. Deprez S, Amant F, Smeets A, et al. Longitudinal assessment of chemotherapy-induced structural changes in cerebral white matter and its correlation with impaired cognitive functioning. J Clin Oncol 2012;30:274–81.
64. Arfanakis K, Haughton VM, Carew JD, et al. Diffusion tensor MR imaging in diffuse axonal injury. AJNR Am J Neuroradiol 2002;23:794–802.
65. Benson R, Meda SA, Vasudevan S, et al. Global white matter analysis of diffusion tensor images is predictive of injury severity in traumatic brain injury. J Neurotrauma 2007;24:446–59.
66. Kraus MF, Susmaras T, Caughlin BP, et al. White matter integrity and cognition in chronic traumatic brain injury: a diffusion tensor imaging study. Brain 2007;130:2508–19.
67. Caeyenberghs K, Leemans A, Geurts M, et al. Brain-behavior relationships in young traumatic brain injury patients: DTI metrics are highly correlated with postural control. Hum Brain Mapp 2010;31:991–1002.
68. Caeyenberghs K, Leemans A, Geurts M, et al. Brain-behavior relationships in young traumatic brain injury patients: fractional anisotropy measures are highly correlated with dynamic visuomotor tracking performance. Neuropsychologia 2010; 48:1472–82.
69. Huisman TA, Schwamm LH, Schaefer PW, et al. Diffusion tensor imaging as potential biomarker of white matter injury in diffuse axonal injury. AJNR Am J Neuroradiol 2004;25:370–6.
70. Niogi SN, Mukherjee P. Diffusion tensor imaging of mild traumatic brain injury. J Head Trauma Rehabil 2010;25:241–55.
71. Focke NK, Yogarajah M, Bonelli SB, et al. Voxel-based diffusion tensor imaging in patients with mesial temporal lobe epilepsy and hippocampal sclerosis. Neuroimage 2008;40:728–37.
72. Powell HW, Guye M, Parker GJ, et al. Noninvasive in vivo demonstration of the connections of the human parahippocampal gyrus. Neuroimage 2004;22:740–7.
73. Concha L, Beaulieu C, Gross DW. Bilateral limbic diffusion abnormalities in unilateral temporal lobe epilepsy. Ann Neurol 2005;57:188–96.
74. Clark CA, Barrick TR, Murphy MM, et al. White matter fiber tracking in patients with space-occupying lesions of the brain: a new technique for neurosurgical planning? Neuroimage 2003;20: 1601–8.
75. Powell HW, Parker GJ, Alexander DC, et al. MR tractography predicts visual field defects following temporal lobe resection. Neurology 2005;23:596–9.
76. Witwer BP, Moftakhar R, Hasan KM, et al. Diffusion tensor imaging of white matter tracts in patients with cerebral neoplasm. J Neurosurg 2002;97: 568–75.
77. Kristo G, Leemans A, Raemaekers M, et al. Reliability of two clinically relevant fiber pathways reconstructed with constrained spherical deconvolution. Magn Reson Med 2013. http://dx.doi.org/10.1002/mrm.24602. [Epub ahead of print].
78. Kuhnt D, Bauer MH, Egger J, et al. Fiber tractography based on diffusion tensor imaging compared with high-angular resolution diffusion imaging with

compressed sensing: Initial experience. Neurosurgery 2013;72(Suppl 1):A165–75.
79. Sherman JH, Hoes K, Marcus J, et al. Neurosurgery for brain tumors: update on recent technical advances. Curr Neurol Neurosci Rep 2011;11:313–9.
80. Pipe JG, Farthing VG, Forbes KP. Multishot diffusion-weighted FSE using PROPELLOR MRI. Magn Reson Med 2002;47:42–52.
81. Holdsworth SJ, Skare S, Newbould RD, et al. Readout-segmented EPI for rapid high resolution diffusion imaging at 3T. Eur J Radiol 2008;65: 36–46.
82. Bammer R, Holdsworth SJ, Veldhuis WB, et al. New methods in diffusion-weighted and diffusion tensor imaging. Magn Reson Imaging Clin North Am 2009;17:175–204.
83. Tournier JD, Mori S, Leemans A. Diffusion tensor imaging and beyond. Magn Reson Med 2011;65: 1532–56.
84. Reijmer YD, Leemans A, Heringa SM, et al. Improved sensitivity to cerebral white matter abnormalities in Alzheimer's disease with spherical deconvolution based tractography. PLoS One 2012; 7:e44074.